# FAST-NEUTRON CODED-APERTURE IMAGING OF SPECIAL NUCLEAR MATERIAL CONFIGURATIONS*

P. A. Hausladen[1], M. A. Blackston[1], E. Brubaker[2], D. L. Chichester[3], P. Marleau[2], and R. J. Newby[1]

[1]*Oak Ridge National Laboratory, Oak Ridge, TN 37830*
[2]*Sandia National Laboratories, Livermore, CA 94551*
[3]*Idaho National Laboratory, Idaho Falls, ID 83415*

## ABSTRACT

In the past year, a prototype fast-neutron coded-aperture imager has been developed that has sufficient efficiency and resolution to make the counting of warheads for possible future treaty confirmation scenarios via their fission-neutron emissions practical. The imager is constructed from custom-built pixelated liquid scintillator detectors. The liquid scintillator detectors enable neutron-gamma discrimination via pulse shape, and the pixelated construction enables a sufficient number of pixels for imaging in a compact detector with a manageable number of channels of readout electronics. The imager has been used to image neutron sources at ORNL, special nuclear material (SNM) sources at the Idaho National Laboratory (INL) Zero Power Physics Reactor (ZPPR) facility, and neutron sources and shielding configurations at Sandia National Laboratories. This paper reports on the design and construction of the imager, characterization measurements with neutron sources at ORNL, and measurements with SNM at the INL ZPPR facility.

## INTRODUCTION

Inspection protocols of future treaties may include technological means of inspection in order to offer additional inspection capabilities (such as identification of nuclear warheads rather than reentry-vehicle-shaped objects) or to enhance inspection confidence (as in instances when only a single warhead would be allowed on a missile designed to carry multiple warheads). One possible use of technological means of inspection would be to count warheads on a missile. The use of fast-neutron emissions to count warheads is potentially desirable because fast neutrons are difficult to shield and, unlike thermal neutrons, directly image the neutron source rather than surrounding moderator. In addition, the use of neutron counting techniques that cannot determine the gamma-ray spectrum emitted by a warhead can lessen the perceived intrusiveness of a potential inspection protocol. On the other hand, the use of fast-neutron emissions effectively limits the use of such a technology to counting items containing materials with a high intrinsic rate of emission, such as plutonium.

Recently, a number of instruments have been developed that are capable of imaging fast-neutron sources based on kinematic reconstruction of interactions of neutrons with charged particles in a

detector [1–3]. These detectors generally have resolutions of order 10 degrees, and as such are unlikely to be useful for counting warheads. While it is difficult to evaluate in detail whether a technology or device is suitable for a task such as counting deployed warheads in a potential future treaty inspection protocol, it is relatively easy to identify basic performance criteria that a detector system must meet in order to be suitable. These criteria can be used to eliminate technologies from consideration that are unlikely to achieve the goal of counting warheads. One such criterion is sufficient angular resolution to count the largest number of warheads that could be present. A "ballpark" value for the required resolution can be estimated by supposing that a missile of diameter $D$ has $N$ warheads mounted in a ring in a single plane in the reentry vehicle. A ring is the space-minimizing geometry for numbers of 6 or less. In this configuration, the distance between warheads is $d = D/(1 + \frac{1}{\sin}(\frac{\pi}{N}))$ for values of $N$ greater than 1. To separate nearest neighbors, the resolution of the imager should be better than 1/2 the inter-warhead distance (preferably better than 1/3). Supposing a missile diameter of 2 m (this represents an average of the four United States and nine Russian intercontinental and submarine launched ballistic missile types recognized by the New START treaty), the spatial resolution required at the missile (assuming the inherent resolution is 1/3 the distance between warheads) is shown in panel (a) of Figure 1. The corresponding angular resolution required when the imager is positioned at reasonable inspection distances of 3, 5, and 10 m away is shown in panel (b).

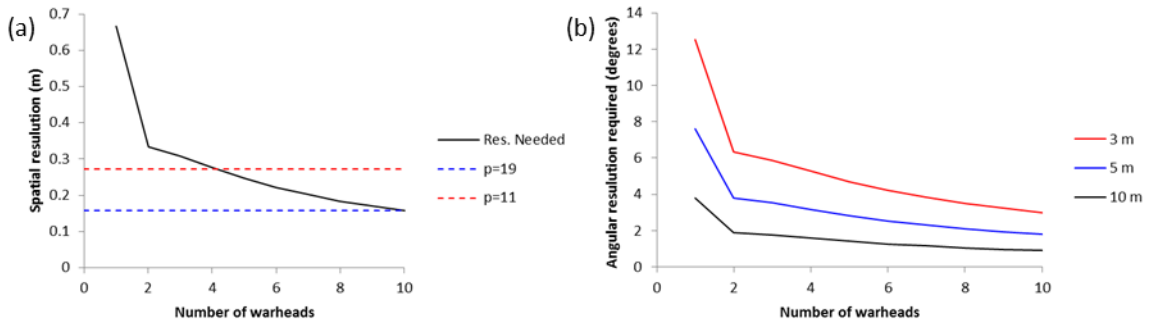


**Figure 1: The (a) spatial resolution and (b) angular resolution required to count warheads for three inspection distances. In panel (a), the dotted lines represent the spatial resolution for imagers with masks of rank 19 and 11 for a 3 m field of view, with no detector subsampling of mask elements included.**

It is worth emphasizing that independent of the actual number of warheads present, the resolution required of the inspection device is that needed to count the largest number of warheads that could be present. As such, in order to count larger potential numbers of warheads from a reasonable distance, angular resolution of a few degrees is required. This requirement largely excludes neutron imaging technologies based on kinematic reconstruction.

In the past year, a fast-neutron imager has been constructed with compact size and sufficient spatial resolution to address potential future treaty confirmation scenarios such as warhead counting. The imager consists of an aperture and a position-sensitive fast-neutron imaging detector whose relative positions are set with a linear stage in order to adjust the field of view [see Figure 2 (a)]. For the measurements reported in this paper, the aperture used was a rank-19 modified uniformly redundant array (MURA) coded aperture constructed of high-density polyethylene (HDPE). Using a rank-19 MURA, the field of view is divided into a 19 × 19 grid of uniquely identifiable basis directions. Consequently, the inherent resolution of such a mask

corresponds to the field of view divided by the mask rank. In the example above, if the field of view of the imager were 3 m, the resulting resolution elements for masks of rank 11 and 19 are shown on the plot of required spatial resolution in Figure 1 (a). For the purposes of warhead counting, a rank-11 MURA may have sufficient resolution, but a rank-19 MURA will have sufficient resolution. A schematic diagram and photograph of the proof-of-concept imager are depicted in Figure 2. In the previous conference proceedings, the design of the proof-of-concept imager was reported [4]. In the present work, performance of the neutron detectors and first imaging results are presented. Results of these first measurements are consistent with the imager having sufficient spatial resolution and efficiency to be capable of counting deployed warheads. Results of measurements of extended neutron sources and shielding configurations are presented elsewhere in these proceedings [5].

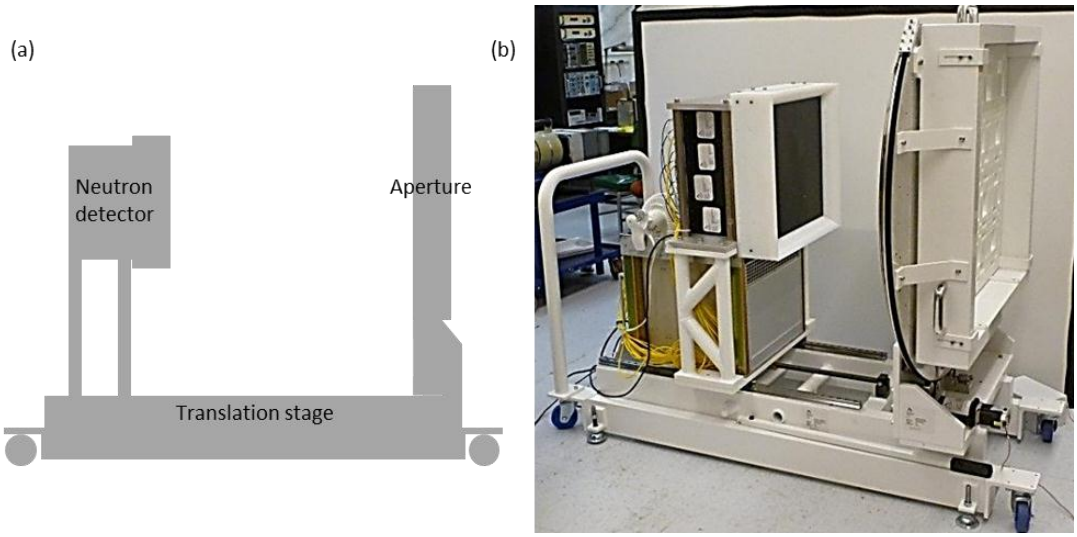


**Figure 2: A schematic diagram (a) and photograph (b) of the fast-neutron coded-aperture imager.**

## PERFORMANCE OF THE NEUTRON DETECTORS

Imaging with pinhole apertures or coded apertures requires a position-sensitive detector plane. For this purpose, pixelated "block" detectors were developed where the active volume of the detectors consists of liquid scintillator EJ-309 [4]. The pixelated detectors instrument a compact detector plane that has a large pixel count and high efficiency with a modest number of readout channels and are able to distinguish between gamma and neutron-induced interactions in the detector. The chosen embodiment of a detector module consists of a 10.4 × 10.4 × 5 cm liquid scintillator volume that is segmented by a reflective grid into a 10 × 10 array of approximately $1 \times 1 \times 5$ cm$^3$ optically isolated pixels of liquid scintillator. The pixels are viewed through a 2.8-cm-thick segmented acrylic light guide by four 51 mm Hamamatsu R9779 fast-timing photomultiplier tubes (PMTs) whose shared response determines the pixel of interaction. The use of a reflector grid to break up the response of the detector into discrete pixels permits uniform position resolution roughly independent of the depth of interaction, thereby enabling use of a thick detector necessary for high efficiency. The reflective grid and container, while minimal, reduce the active area of the detector to 82% of its total area. The detectors are modular, and the detector plane of the imager is made up of 16 neutron and gamma-ray detectors arranged in a 4 × 4 array. Together, the detectors comprise a 43 × 43 cm panel of 1600 pixels.

In the present implementation, readout of the four PMT signals of each detector is accomplished using four channels of an XIA Pixie-16 12-bit 100 $MSs^{-1}$ waveform digitizer. In part, the XIA system is used because it is possible to trigger synchronous digitization of four channels with the sum signal to support correct position calculation. The signal presented to each channel of waveform digitizer corresponds to a PMT anode pulse integrated on a preamplifier to yield a charge pulse with a relatively short decay time (2.5 μs). This analog integration was performed to avoid missing the contribution of individual photoelectrons in the signal because the height or duration was too small to be recorded by the dynamic range or band pass of the digitizer. A plot of two representative charge pulses, one from a gamma ray (red) and one from a neutron (blue), is shown in Figure 3.

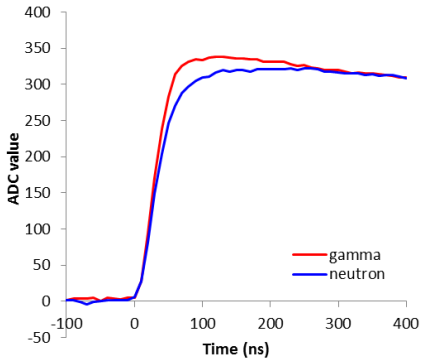


**Figure 3: Measured waveforms for gamma rays and neutrons.**

The amplitudes of the four PMT signals are used to calculate the pixel of interaction. The shape of the summed signal of the four PMTs is used to determine whether the interaction involved a neutron or gamma ray. While the full waveform of the pulse could be used, most of the information that is present in the waveform can be summarized in a few points. For instance, for a pulse with given amplitude at 400 ns, the maximum difference between gamma and neutron-induced pulses is in the waveform sample at 70 ns (refer to Figure 3). In the present system, samples are recorded at 70 and 400 ns and also at 80 and 410 ns. The nearby points are recorded because individual waveforms are not synchronized with the clock of the digitizer, and interpolation between the two values based on the actual timing provides somewhat improved pulse-shape discrimination (PSD). An average digitizer value for the baseline is also necessary for baseline subtraction. Using data recorded in this way, the position response of the detector to uniform illumination by neutrons emitted from a deuterium-tritium (D-T) neutron generator can be seen to the right in Figure 4. Likewise, the pulse shape (vertical coordinate) as a function of pulse height (horizontal coordinate) is shown to the left in Figure 4. To aid the eye, a boundary is drawn on the pulse-shape plot around neutron events that includes counts that are within 2 standard deviations of the average neutron response and excludes counts that are within 4 standard deviations of the average gamma response.

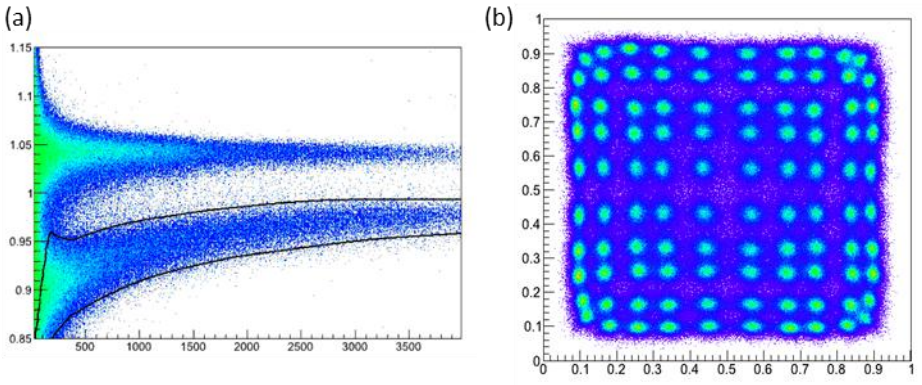


**Figure 4: Measured (a) pulse shape and (b) position response of a detector to 14 MeV neutrons. Pulse shapes consistent with neutrons are indicated by the black boundary.**

The performance of the imaging system depends on many factors, but the most basic of these factors is the ability of the imaging system to correctly identify the type of particle (e.g., neutron or gamma ray) and the pixel of interaction when an interaction of an incident particle gives rise to a set of signals in the four PMTs of a constituent detector. The limits of detector performance are primarily determined by photon counting statistics and properties of the scintillator. In addition to limitations imposed by photon counting statistics, limitations to pulse-shape performance were analyzed from a variety of sources including the dynamic range, noise properties, band pass, and timing properties of the waveform digitizers; variability in light collection in the individual detector pixels; and after-pulsing in the PMTs. The quality of pulse-shape discrimination was calculated in terms of the usual figure of merit (FOM), namely, the difference between the centroids of the gamma and neutron distributions divided by the sum of their full widths at half maximum (FWHMs). In Figure 5, the actual performance of the detectors is compared to that calculated based on the measured light yield and pulse shapes for scintillator EJ-309, variance in single-photon amplification in the PMTs, and properties of the digitizer.

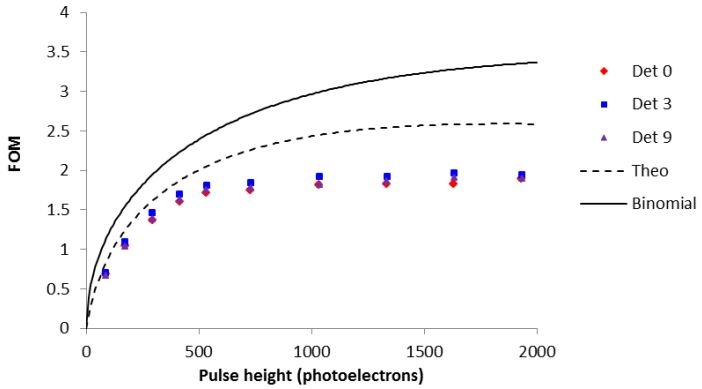


**Figure 5. Expected and measured neutron-gamma separation. The solid line corresponds to the limit corresponding solely to counting statistics, while the dashed line also includes single-photon amplification variance, digitizer root mean square error, and timing misalignment between the source pulse and digitizer clock. The remaining discrepancy between measured points and the prediction originates in PMT after-pulsing.**

Note that the measured quality of pulse-shape determination falls short of that calculated by approximately 25%. Further investigations indicated that most of this discrepancy originates

from PMT after-pulsing. For a pulse of given amplitude, a typical PMT exhibits after-pulsing manifested as discrete pulses arriving within approximately 10 μs of the original pulse and corresponding to an average integrated yield of approximately 3–4% of the original pulse amplitude. These pulses skew the pulse-shape measurement, specifically putting a tail on gamma events tending toward neutron events. An example oscilloscope trace of a PMT anode pulse showing after-pulsing in addition to the train of photoelectrons can be seen in Figure 6.

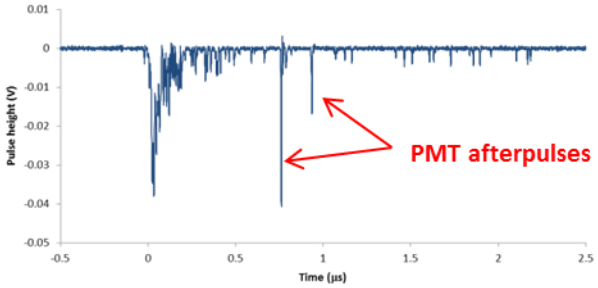


**Figure 6. A PMT anode pulse showing large after-pulses visibly identifiable amount single photoelectrons.**

With the present detector performance, the imager achieves sufficient neutron-gamma separation at 1.1 MeV proton recoil, 90% of neutrons are separated from the average gamma rays shape by more than five standard deviations. Further improvements in the quality of PSD will make gamma-ray rejection at a higher level possible or will make modest improvements in the efficiency of the detector possible through allowing discrimination on lower-energy neutrons. For example, if discrimination could be performed for interactions producing half the collected light as at present, the efficiency of the detector would be increased roughly 10% for $^{252}$Cf spectrum neutrons over the present intrinsic efficiency which exceeds 20%. This improvement in efficiency would allow measurements to be performed 20% faster.

At the outset of this work, liquid scintillators were the only scintillators commercially available in suitable quantities that had PSD properties. The use of liquid scintillator brings with it a number of technical challenges associated with the solvent action of the liquid scintillator and its thermal expansion and contraction. Foremost among these challenges is the inherent differences in expansion coefficients (with temperature) for the acrylic window and aluminum housing of the liquid scintillator cell. This difference makes the detectors fragile to temperature changes that are relatively modest (e.g., departure from room temperature by more than 20° F), making them a good laboratory device but not suitable for fielding to environments that are not temperature controlled, even for short durations or during storage. Effort is under way to replace the liquid-based detectors with detectors constructed from the newly available plastic scintillators with PSD capability [6]. In these new detectors, PMTs designed for an order of magnitude less after-pulsing will result in improved PSD performance.

## IMAGING MEASUREMENTS

Following assembly of the imager and calibration of the detectors, an initial imaging measurement was performed at ORNL of a neutron source configuration comprised of a set of five $^{252}$Cf sources. A (a) photograph of the imager, a (b) photograph of the configuration of sources, the (c) modulated counts on the detector, and the (d) reconstructed image can be seen in Figure 7. Note that the closest two sources are separated by 10 cm. For a base-19 MURA coded

aperture mask, the position of the open portions of the mask and closed portion of the mask are interchanged through rotation of the mask by 90 degrees. The two configurations are known as "mask" and "anti-mask," respectively, and imaging based on the difference eliminates backgrounds that are not modulated by the mask. For this image, data was taken using a 7.2 cm thick HDPE mask whose smallest element was 1.4 cm. The mask was located 111 cm from the sources, and the detectors were positioned 67.3 cm from the mask. Data was taken for both the "mask" and "anti-mask" configurations of the coded aperture for a measurement time totaling 1 hour. The $^{252}$Cf sources are each identical in strength at approximately 40,000 neutrons per second. In addition to the two-dimensional image, a one-dimensional slice was made through the image along the vertical line going through the two closest sources, and this slice is shown in (e), where the resolution in centimeters has been converted to an angular resolution. Fits to the sources in this slice found them to be separated by 3.5 degrees with root mean square widths of 0.7 degrees (FWHMs of 1.8 degrees). The plot shows that the imager is capable of high-resolution images similar to what is expected to be necessary to count warheads.

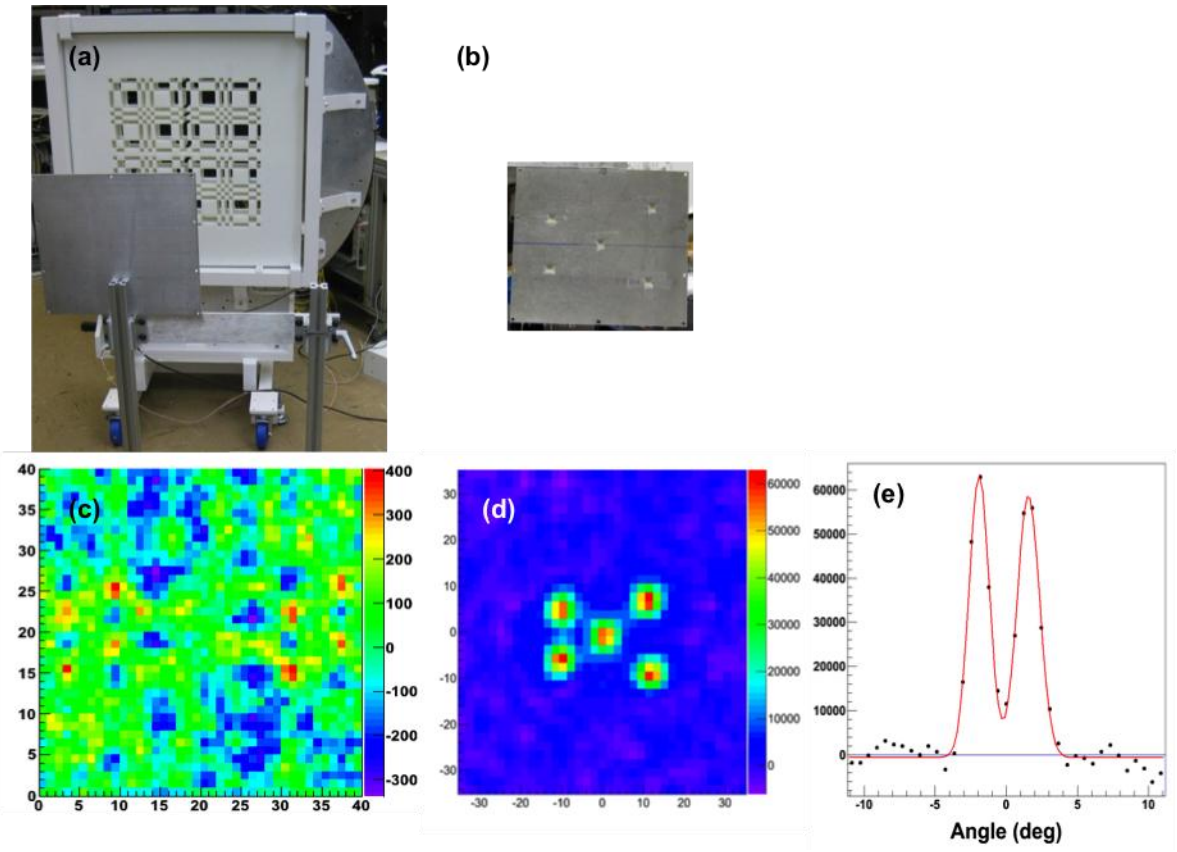


**Figure 7. The first image at ORNL with $^{252}$Cf sources. The imager can be seen (a) during measurement of the (b) configuration of five $^{252}$Cf sources where the closest two sources are separated by 10 cm. The difference between the distribution of counts in the "mask" and "anti-mask" configurations is shown in (c), while the reconstructed image is shown in (d). In (e), a slice through the image along the line including the closest two sources shows the angular resolution to be 1.8 degrees.**

At the INL ZPPR facility, calibration of the detectors and initial exercising of the imaging system was performed with a D-T neutron generator. The D-T source was useful for this purpose because it is an intense source, the source is point like, and the neutrons are high energy. Two configurations of the D-T generator were measured, one centered and one off center. One

of these configurations along with the modulated counts on the detector for each configuration and the reconstructed images can be seen in Figure 8. For these measurements (and the rest of the measurements at ZPPR), a 7.2 cm thick HDPE mask with a smallest aperture size of 1.4 cm was used. The mask was located 100 cm from the D-T generator target, and the mask-detector separation was 61 cm.

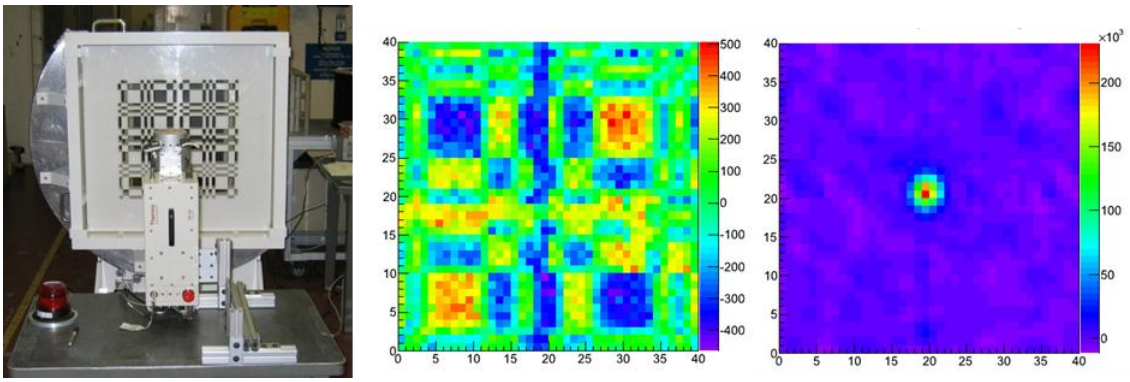

**Figure 8. Initial calibration imaging measurements of a point source consisting of a D-T generator roughly centered in the field of view.**

After initial calibration measurements, several of the "Inspection Objects" (IOs) available at the ZPPR facility were imaged. These inspection objects gave an opportunity to perform measurements with kilogram quantities of special nuclear material (SNM), including weapons-grade plutonium and highly enriched uranium (HEU), and are described in detail in [7]. In particular, IO #9 was measured in isolation, and IOs #7 and #10 were measured side by side. The setup for the measurement of IO #9 can be seen in (a) and (b) of Figure 9. A photograph of the six-sided box of SNM with external dimensions of approximately 10 cm on a side can be seen in panel (e). This IO has 96 g of $^{240}$Pu in it, so it has an intrinsic rate (prior to multiplication) of about $10^5$ neutrons per second. The measurement period for the image shown corresponds to 1 hour each of the mask and anti-mask configurations. The modulated counts corresponding to the mask data minus the anti-mask data are shown in panel (c), while the reconstructed image of the neutron source is shown in (d). In comparison to the earlier images of the point-like $^{252}$Cf and D-T neutron generator sources, this source is identifiably larger than a point source. As indicated earlier, the highest resolution mask available for the measurement had a minimum aperture size of 1.4 cm. With this aperture size, in order that at least an entire base-19 pattern is projected onto the detector, the image will be smaller than the object by at least a factor of 0.6. Consequently, a 10 cm neutron source will project on 6 pixels. With this resolution, it is clear that the neutron source is not point like. However, note also that the resolution of this image is insufficient to see details of the SNM box, such as the wall thickness.

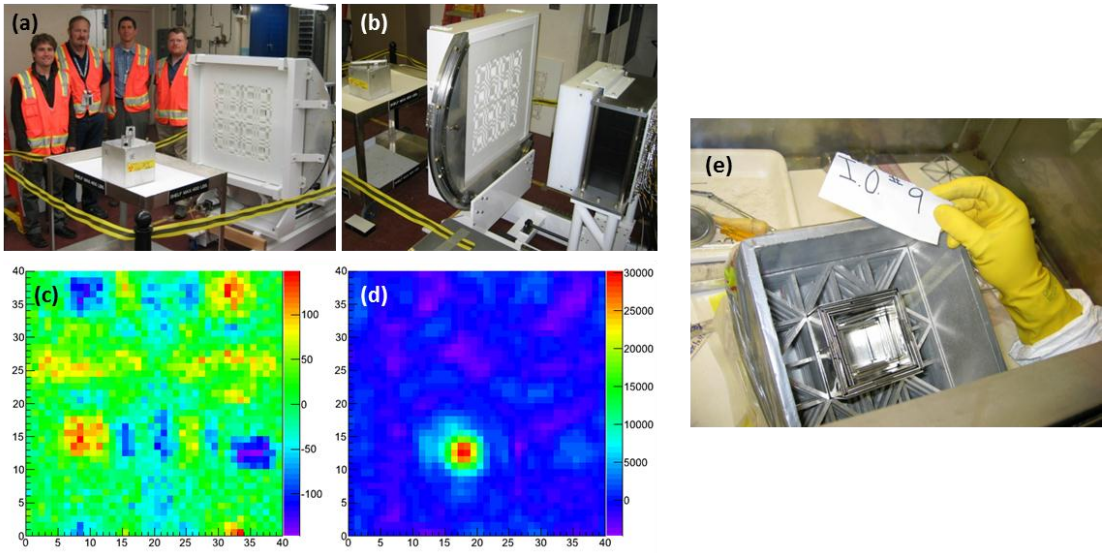


**Figure 9. Photographs (a) and (b) of the measurement configuration containing (e) IO #9, shown here under construction. The (c) modulated counts on the detector are processed to get (d) the fast-neutron image.**

A second measurement was performed with IO #10 next to IO #7. IO #10 also contains 96 g of $^{240}$Pu, but this neutron source is moderated by 5 cm of polyethylene shielding. IO #7 contains 5.25 kg of HEU, so the thermalized flux of neutrons from IO #10 would induce some fission in IO #7 that could potentially be seen as a separate fission source. The measurement configuration can be seen in (a) Figure 10, along with (b) a photograph of the IO #10 during its assembly. While the purpose of the HDPE aperture is to modulate neutrons, it also modulates gamma rays. Consequently, the neutron imager can be used as a gamma imager that is incapable of spectroscopy. Panel (c) shows the modulated gamma counts on the detector, while panel (d) shows the modulated neutron counts on the detector. The corresponding gamma-ray and neutron images (from the point of view of the imager) are shown in panels (e) and (f), respectively. Note that IO #10 shows up as a combined gamma and neutron source, while IO #7 shows up only as a gamma-ray source. The measurement period for the image shown corresponds to 1 hour each of the mask and anti-mask configurations. Potentially because of neutron scattering, the image of the moderated plutonium source appears larger than the previous measurement of an unmoderated source. Equally interesting, the HEU in IO #7, which has a negligible spontaneous neutron emission rate for the purposes of imaging on realistic time scales, also does not have a sufficiently high induced neutron emission rate (due to neutron-induced fission) to be visible in a reasonable measurement period of 1 hour; in this measurement, identifying the induced fissions with a signal to noise of 5 would have taken 6 times longer.

While sources with a low intrinsic neutron emission rate will be difficult to image, for sources with high intrinsic rates (such as plutonium), the high resolution and high efficiency possible with the coded-aperture technique are amenable to the application of warhead counting.

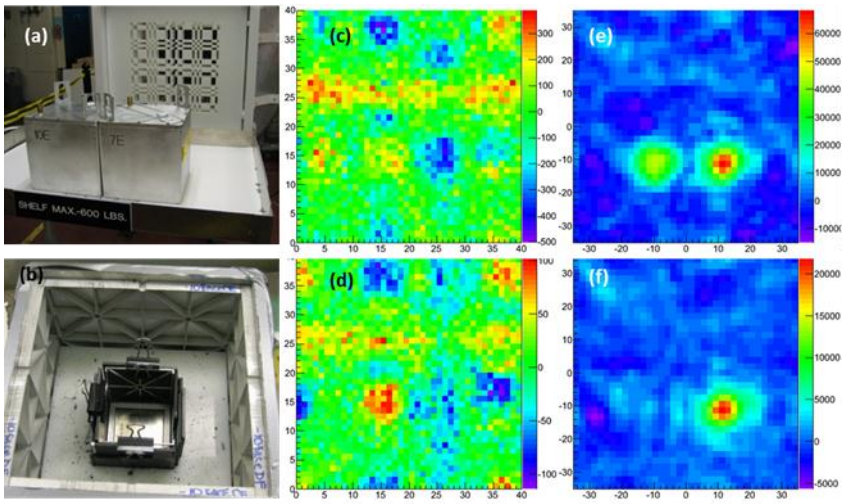


**Figure 10. Photographs (a) of the measurement configuration with IO #10 and IO #7 and (b) of IO #10 shown here under construction. The (c) modulated gamma-ray counts and (d) modulated neutron counts on the detector are processed to get (e) the gamma-ray image and (f) the fast-neutron image.**

## ACKNOWLEDGEMENTS

This research is supported by the US Department of Energy National Nuclear Security Administration Office of Nonproliferation and Verification Research and Development and Office of Nuclear Verification. It is also supported by US Department of Energy Office of Nuclear Energy as part of the Fuel Cycle R&D MPACT campaign.

## REFERENCES

1. I. Jovanovic et al., "Directional Neutron Detection Using a Time Projection Chamber," IEEE Transactions on Nuclear Science, 56, p. 1218, 2009.

2. G. A. de Nolfo et al., *Neutron Imaging Camera*, IEEE Nuclear Science Symposium Conference Record, 282, 2008.

3. N. Mascarenhas et al., *Results with the Neutron Scatter Camera*, IEEE Transactions on Nuclear Science, 56, p. 1269, 2009.

4. M. A. Blackston et al., "Fast Neutron Coded-Aperture Imaging for Warhead Counting," 52nd Annual Meeting of the Inst. of Nucl. Materials Mgmt., 2011.

5. P. Marleau et al., "High-Resolution Imaging of Fission Energy Neutrons," 53nd Annual Meeting of the Inst. of Nucl. Materials Mgmt., 2012.

6. N. Zeitseva et al., "Plastic scintillators with efficient neutron/gamma pulse shape discrimination," NIM A, 668, p. 88, 2012.

7. R. Neibert et al., *Passive and Active Radiation Measurements Capability at the INL Zero Power Physics Reactor (ZPPR) Facility*, INL/EXT-11-20876, 2010.